Electromagnetic pulses, optical emission and chemical change associated with high-power laser-induced dielectric breakdown of gaseous sulphur hexafluoride

Veronika Horká-Zelenková[1,*], Josef Krása[1], Martina Toufarová[1], Jakub Cikhardt[2,3], Pooja Devi[1,4], Shubham Agarwal[1,4], Norbert Kanaloš[1,5], David Ettel[1,6], Roman Dudžák[1,3], Tomáš Burian[1], Michal Krupka[1,3,5], Jan Novotný[2], Sushil Singh[1,2,3], Libor Juha[1]

[1] *Institute of Physics of the Czech Academy of Sciences, 18200 Prague, Czech Republic*

[2] *Czech Technical University in Prague, Faculty of Electrical Engineering, 16627 Prague, Czech Republic*

[3] *Institute of Plasma Physics of the Czech Academy of Sciences, 18200 Prague, Czech Republic*

[4] *Charles University in Prague, Faculty of Mathematics and Physics, 18000 Prague, Czech Republic*

[5] *Czech Technical University in Prague, Faculty of Nuclear Science and Physical Engineering, 11519 Prague, Czech Republic*

[6] *Technical University of Liberec, 46117 Liberec, Czech Republic*

Abstract

A large laser spark was produced in a homogeneous sulphur hexafluoride gas (pressures ranged from 10.7 to 101.3 kPa) by a focused high-power laser pulse (350 ps, 125 J, 1315.2 nm). Magnetic fields, electromagnetic pulses (EMP), optical emission spectra (OES) and chemical changes associated with the laser-induced dielectric breakdown (LIDB) in the SF_6 gas were investigated. During the laser interaction, hot electrons escaping the plasma kernel produced EMP and spontaneous magnetic field, the frequency spectrum of which contains three bands around 1.15, 2.1 and 3 GHz, while the EMP frequency band appeared around 1.1 GHz. The EMP emission from a laser spark was very weak in a comparison to those generated at a solid target. Gas chromatography revealed the

This peer-reviewed article has been accepted for publication but not yet copyedited or typeset, and so may be subject to change during the production process. The article is considered published and may be cited using its DOI.

10.1017/hpl.2025.10061

formation of only a limited number of products and a low degree of sulphur hexafluoride (SF_6) conversion. OES diagnosed the LIDB plasma in phase of its formation as well as during its recombination.

Correspondence to: V. Horká-Zelenková, Institute of Physics of the Czech Academy of Sciences, 18200 Prague, Czech Republic. Email: zelenkova@fzu.cz

Keywords: laser spark, electromagnetic pulses, sulphur hexafluoride, gas chromatography, optical emission spectroscopy.

1. INTRODUCTION

Electromagnetic pulses (EMP) emitted by laser-produced plasma represent an extensively studied phenomenon. Numerous results have been obtained studying the interactions of high-power laser radiation with solid targets. The study of EMP from plasmas created by focusing a laser beam into a homogeneous gas (laser spark) has been the subject of a few articles so far. This is surprising because laser sparks, if generated under the properly chosen conditions (i.e., absence of metallic parts of the gas cells), make it possible to study the EMP phenomena associated only with the plasma, unaffected by a solid target, its holder and vacuum interaction chamber.

The molecular gas, chosen for performing the interaction experiments reported in this article, is sulphur hexafluoride. There are several good reasons for this choice. At the beginning of the last century, Henri Moissan and Paul Lebeau [1], the French chemists, synthetized an extremely stable compound from two highly reactive elements, fluorine and sulphur. The high stability of SF_6 is due to strong S-F bonds and a perfect octahedral symmetry of the molecule (Figure 1). Sulphur hexafluoride has also unique electrical properties, e.g., a high electron affinity [2,3]. In science and technology, numerous disciplines (see, please, refs [4-11] and numerous references

https://doi.org/10.1017/hpl.2025.10061 Published online by Cambridge University Press

cited therein) benefit from the exceptional properties of this molecule, e.g., biomedicine (anaesthesia; magnetic resonance imaging; gas tamponade; ultrasound contrast agent), chemical industry and metallurgy (non-reactive gas with a high heat capacity; blanketing gas), chemical, especially photochemical synthesis (fluorination agent), laser science and engineering (insulating and buffer gas; reactant in chemical lasers; sensitizer in infrared laser chemistry), nuclear industry (insulating gas; tracer; leak indicator), radiation, flame and plasma sciences (electron scavenger), microchip production (plasma etching), environmental and earth sciences (tracer), etc. However, it has reached its widest spread in the electric power industry serving as a gaseous dielectric, insulating gas in high-voltage devices, especially switches, circuit breakers. Unfortunately, SF_6 molecules exhibit a strong absorption in the mid-infrared spectral range. It is therefore a gas that contributes significantly to the greenhouse effect in the atmosphere. Thus, the new source of motivation [12] appeared for the study of SF_6 plasma-chemical reactivity. Not only the possibilities of replacing it completely, but also of recycling it or mixing it with other gases are being studied.

Figure 1 Ball and stick model of sulphur hexafluoride.

It follows from the brief overview given above [1-12] that SF_6 represents a unique compound with numerous applications. Nevertheless, there is also a very strong motivation for its choice to be investigated at the PALS facility directly in the field of laser-plasma chemistry, since the first attempts to elucidate the chemical consequences of laser-induced breakdown of gaseous SF_6 appear already in 70s [13,14]. These papers are only two, but they contain very interesting findings that need to be confronted with results obtained using the new approaches and experimental possibilities offered by high-power lasers. The first [13] describes the strong influence of the inner surface of the gas cell. In the present work, it is eliminated by the larger dimensions of the gas cell and only a low number of accumulated high-energy pulses. The latter

https://doi.org/10.1017/hpl.2025.10061 Published online by Cambridge University Press

[14] discerns between two mechanisms that control the chemical reactions initiated by the LIDB plasma at different pressures. At pressures below 2.7 kPa, the decomposition yields are controlled by the rate constants of non-thermal processes associated with electron attachment to SF_6 molecule, which has uniquely high electron affinity (see ref. [2] and numerous references cited therein), while the contribution of thermal decomposition raises with increasing gas pressure. At pressures exceeding 6.7 kPa, pyrolysis dominates the decomposition processes.

A specific source of electromagnetic pulses (EMPs), which are characterized by a short burst of electromagnetic energy, is plasma produced by the interaction of a laser pulse with a solid target or gas [15]. The power, duration, and frequency range of the EMP depend on the properties of the plasma and its environment, such as the interaction chamber or surrounding gas. The EMP intensity rises steeply to a maximum and then decreases more slowly. It usually has a shape of a damped sinusoidal pulse. EMPs, which are regularly detected during the interaction of femtosecond to nanosecond laser pulses with matter, are generally considered a threat to electronic devices and diagnostics and have prompted the development of various protective measures [16, 17]. The EMP spectrum generally spans many frequency bands, from tens of MHz to the terahertz limit. The electromagnetic fields of EMPs are of primary importance not only for the safe operation of high-power and high-energy laser devices, but also for the possible application of these electromagnetic fields [15].

The EMP is primarily driven by the most energetic electrons being able to pass through the plasma potential barrier (of a virtual cathode) and to escape the laser-produced plasma [18]. When laser interacts with a solid, the escape of electrons causes positive charging of the target [19,20]. This charge is neutralized by a return current flowing between the target and the interaction chamber through the target holder [21]. As this current oscillates, the target holder becomes an antenna emitting the EMP in the GHz domain. Additionally, the geometry of the interaction chamber determines the MHz domain of the EMP spectrum because the electrons

https://doi.org/10.1017/hpl.2025.10061 Published online by Cambridge University Press

from the evaporating target striking the chamber walls cause the chamber to resonate at its fundamental and resonant EM frequencies [22].

Ultrashort high-intensity laser pulses focused on a metal foil, or a gas can generate terahertz radiation, which has been intensively studied experimentally and theoretically for applications in various fields [23-26]. A comparison of the EMP frequency spectra emitted by plasmas produced in gases and on metal targets shows that, despite the different mechanisms of expansion of electrons into the gas surrounding the plasma core, EMP frequencies can be assigned to the same frequency bands, especially the ultra-high frequency (UHF) band ranging between 0.3 – 3 GHz. Primarily, megahertz and gigahertz frequency of EMPs are generated not only in various high-power laser experiments but can also be generated by flashes of hard X-rays emitted from nuclear explosions in the air, high-energy explosives, as well as partial discharges in high-voltage (HV) systems [27-30].

A similarity between EMP generated by a laser spark and partial discharges can be seen because the observed broadband UHF spectra match to the short duration of the produced filaments or sparks. For example, the observed electronic part of the partial discharge can have a pulse rise time of 0.3 to 0.8 ns and a FWHM (full width at half maximum magnitude) duration of about 1.5 ns [31]. Femtosecond lasers can produce EMPs with durations longer than 100 ps, but the lifetime of the laser plasma kernel can reach tens of nanoseconds. [32]. Although data on EMPs produced by nanosecond lasers are sparse, time-resolved spectral and shadowgraph imaging of sparks demonstrate long plasma kernel duration of up to hundreds of microseconds [33].

A laser driven UHF radiation from an under-dense gas plasma is much weaker than from a solid target, which is grounded. In our case, electrons escaping from the plasma kernel are not only slowed down by collisions with surrounding cold gas particles, but if they approach the inner surface of the gas cell, they do not reach the ground, as they are insulated from it by both

https://doi.org/10.1017/hpl.2025.10061 Published online by Cambridge University Press

the cell and the electrically non-conductive holder of the cell. This indicates that the source of the EMP is the plasma kernel itself. Although the question of the origin of the EMP arising from the interaction of a laser pulse with gas has not yet been fully answered, it is nevertheless inclined to the idea that the EMP is generated by electric currents in plasma [34].

The cold ambient gas is ionized not only by the hot electrons, but also by X-rays and extreme ultraviolet radiation from the plasma kernel. As a result, the ambient gas is transformed into a low-temperature plasma. This phenomenon has been investigated by Bartnik et al. in SF_6 using an external laser-plasma source of XUV radiation [35]. Finally, a shock wave is generated, and further ionic and atomic species are formed revealed by their emission in the ultraviolet and visible regions of the electromagnetic spectrum [33, 36]. Thus, the experiments also provide useful insights in the spark chemistry with respect to differences in laser absorption properties.

In this article, we present the results of an EMP experiment conducted on the iodine photodissociation laser system PALS, which operates at a wavelength of 1315.2 nm [37]. The laser pulses with an energy of about 120 J and a length of 0.3 ns were focused into a gas cell, which does not contain any metal component, filled with SF_6. In addition to EMP, we also focused our attention on the emission of near-ultraviolet and visible radiation in the wavelength range of 300 - 700 nm and on identification of products formed in reactions initiated by LIDB plasmas.

2. EXPERIMENTAL SETUP

A glass cell of simple design has been used to generate laser sparks in various gases. The cell features a cylindrical body with an external diameter of 90 mm and a length of 250 mm and BK7 glass window with the following parameters: thickness of 15 mm and diameter of 98 mm for laser beam entry (see figure 2). This window has an antireflective coating and is mounted to the cell using a two-part Murytal® flange. The front section of the flange is machined as a

https://doi.org/10.1017/hpl.2025.10061 Published online by Cambridge University Press

single piece with an internal thread, while the rear section consists of two interlocking pieces, allowing it to be positioned over the cell collar. The Murytal® material provides high rigidity and strength, ensuring that all components are precisely manufactured for a secure fit and preventing thread damage. Moreover, it is chemically resistant. To ensure mechanical integrity, the flange system incorporates a triple-sealing arrangement. Teflon® gasket protects the window from mechanical damage, an NBR rubber gasket shields the cell collar during closure, and a highly chemically resistant Kalrez® O-ring provides a tight seal between the cell collar and the window.

The entire cell assembly is mounted in a three-dimensionally printed polymer socket, which is attached to a Murytal® holder. Both the socket and holder are fabricated from non-conductive polymeric materials, ensuring electrical isolation from ground. A vacuum line is connected to the cell, enabling precise control of sample pressure and concentration, as well as efficient extraction of reaction products following laser irradiation. These products are immediately analyzed using gas chromatography– mass spectrometry (GC-MS). The laser beam [37] was focused into the centre of the gas cell by a lens with a focal length of 300 mm (see Figure 3 for details).

Figure 2 Gas cell.

The fibre optic spectrometer HR4000 by Ocean Optics was used to record the emission spectra. The spectrometer has detection range between 200 nm and 1100 nm and uses a 3648-element linear silicon CCD array allowing for spectral resolution of 0.75 nm FWHM. The light from the laser spark was collected using the optical fibre facing the spark at a distance of 25 cm and no collimating optics were used. Time-integrated photography of the glowing spark was performed using a CCD camera TM-4200 GE.

https://doi.org/10.1017/hpl.2025.10061 Published online by Cambridge University Press

A double-ridged waveguide horn antenna Rohde & Schwarz HF907 with a bandwidth of 0.8-18 GHz was placed at angles of 55° to the laser axis. The antenna mount made it possible to change the antenna orientation and measure both the vertically and horizontally polarized EMPs in the identical point. A loop probes RS H 400-1 of 2.5 cm in diameter were used to detect near H-filed ranging from 5 to 3000 MHz. The antenna and loops were adjusted so that their directionality maximum was oriented towards the discharge gap centre, and the polarization of each magnetic loop approximately coincides with the direction of the discharge gap axis. The layout is shown in Figure 3.

Figure 3 Schematic of experimental setup.

3. EXPERIMENTAL RESULTS AND DISCUSSION

3.1. Magnetic probe signal

In general, the plasma produced by a laser is a source of spontaneous magnetic field [38]. Perhaps the first measurement of this field was performed in a spark plasma by V.V. Korobkin and R.V. Serov [39] and a simple model of laser spark plasma formed by the mechanism of delayed breakdown in the focal cone of a focused ns laser beam in gas was proposed by Yu. P. Raizer [40]. Regarding the self-generating electric and magnetic fields around a laser spark, K. Rohlena and M. Mašek presented an assessment of various models of spark formation and their comparison with experimental findings [41].

In our experiment, the spontaneous magnetic field was detected 10 cm from the laser focus using a loop magnetic probe type RS H 400-1 with a diameter of 25 mm. Its orientation allowed to record the time derivative of azimuthal magnetic field $\dot{B}_\varphi$ induced by the pulsed electric current flowing through the plasma core, as shown in Figure 4. Please note that $\dot{B}_\varphi$ is a part of the total detected $\dot{B}$ which also includes the contribution of the EMP field also detected by the horn antenna 2.5 m from the spark, as described in Section 3.2. Figure 4a compares the time course of 6 probe signals S_{RS} together with the time course of the laser intensity, I_L, where I_L is synchronized with the S_{RS} in such a way that the I_L peak matches the highest positive peak of S_{RS} appearing at time 1 ns. The dominance of the second positive peaks of S_{RS} is evident. Once the interaction of the laser pulse with the gas stops, the magnetic field quickly disappears,

https://doi.org/10.1017/hpl.2025.10061 Published online by Cambridge University Press

causing a rapid reduction in the energy supply to the probe, as shown in Figure 4b. This energy was calculated using the relationship:

$$E_{RS} = \int S_{RS}^2/R \; dt, \tag{1}$$

where R is the load impedance given by the coaxial cables and oscilloscope input. Please note that $E_{RS}(t)$ reaches a level of 46% of the maximum value approximately already in 0.5 ns.

Figure 4 Electromagnetic radiation detected with the magnetic probe.

The short-time Fourier transform (STFT) with a Hanning window and an overlap of 22 of the $S_{RS}(t)$ signal presented in Figure 4c shows that the probe signal oscillates from 0.2 to 5 GHz, with three frequency bands dominating around 1.4, 2 and 3.2 GHz.

The used window size of ≈1/3 ns, corresponding to the full width at half maximum of the laser intensity, reveals a broadband spectrum in the range from 1 to 3 GHz with a maximum at ≈2 GHz at ≈0.5 ns. This time correlates with the maximum of the laser pulse, as shown in Fig. 3a, and therefore the frequency of ≈2 GHz could be considered as the frequency of the magnetic field generated primary around the laser spark during the interaction of the laser pulse with the gas. This magnetic field is generated by the standard mechanism of crossed electron density (n_e) and temperature (T) gradients ($\partial\vec{B}/\partial t \sim n_e^{-1}[grad\, T \times grad\, n_e]$), while the electric field is supposed to be created by the polarization of the plasma due to its radial expansion across the self-generated magnetic field [41]. Thus, the magnetic probe signal reveals two sources of the electric and magnetic fields. One is the laser pulse itself, which, through electron density and temperature gradients, generates the observed azimuthal magnetic field, B_φ, winding around the spark plasma, whereas the electric field with $E_\varphi = 0$ is induced by a charge separation, i.e. polarization of the plasma streaming radially across the self-generated magnetic field. We note that the B_φ field is detected just during the interaction of the laser with the gas, see Figure 4a and c.

Assuming that the magnetic flux density B_φ is constant within the probe's effective area A_{ef}, the output voltage can be calculated as:

$$S_{RS} = -A_{ef}\, G\, \frac{dB}{dt}, \tag{2}$$

where G is the attenuation of the probe, specified in the manufacturer's datasheet [42] as −25 ± 5 dB (a factor of ≈ 0.056) within the frequency range of 200–1000 MHz. The current inducing the magnetic field in the magnetic probe can be evaluated by the integration of the near field probe signal S_{RS} which is proportional to the time derivative of B_φ:

https://doi.org/10.1017/hpl.2025.10061 Published online by Cambridge University Press

$$J_{RS}(t) = -\frac{1}{M}\int S_{RS}(t)dt, \quad (3)$$

where M is the conversion coefficient representing the mutual inductance between the magnetic loop and the laser spark (conducting plasma kernel). By combining Eq. (3) with Eq. (2) and Ampère's circuital law, we obtain:

$$J_{RS}(t) = -\frac{2\pi r}{\mu_0}\frac{1}{A_{ef}G}\int S_{RS}(t)\,dt, \quad (4)$$

where *r* is the distance of the B-field probe from the laser spark. An example of the time course of $\int_0^t S_{RS}(t)dt$ is shown in Figure 5. As shown, the magnetic flux density peak reaches several tens of μT.

Figure 5 S_{RS} signal and its integral.

Using the PALS laser, estimated values of magnetic field intensity near the tip of the plasma can reach 0.1 T values and the intensity of the accompanying electric field can be in the range of 100 V/cm [41]. Another source of electromagnetic field are the gradients of the laser spark, which persist in a short-term self-sustaining plasma inside the spark without being actively driven by the laser pulse, as will be elucidate in Section 3.2. Please note the frequency band around 1.4 GHz, which later appeared in the STFT only after the occurrence of 2 GHz at 1 ns (see Figure 4c), is the only one that dominates the far zone where the horn antenna detects the EMP, see the S_{HA} signal shown in Figure 6.

Please note that in this case the probe signal is induced not only by non-radiating currents, but also by emitted EMP. Since the value of *M* is time independent, it can be deduced that the integral of the bipolar signal $S_{RS}(t)$ results in a bipolar time course of the current $J_{RS}(t)$. We note that only exceptionally was an almost unipolar $J_{RS}(t)$ waveform obtained. According to Eq. (3) and magnetic field $B(t)$ shown in Fig. 4, the peak of the current $J_{RS}(t)$ reaches tens of amperes and a carried charge of a few nanocoulombs.

3.2. Horn antenna signal

Sparks produced by a single NIR laser pulse carrying an energy of 126±4 J focused into a cell filled with SF_6 at a pressure of 10.7-101.3 kPa emit EMPs, as shown in Figure 6. The horn antenna was placed 2.5 m far from the laser spark at an angle of 55° to the laser vector. Figure shows a series of signals, S_{HA}, obtained by repeating firing into a SF_6-filled cell. Figure 6a also shows the time course of a laser pulse, where the first positive peaks of the signals S_{HA} of the horn antenna matching the peak of the laser intensity. The time course of the EMP emission can be characterized by the variation of the energy absorbed by the horn antenna, as shown in Figure

https://doi.org/10.1017/hpl.2025.10061 Published online by Cambridge University Press

6b for the shot 61812. This energy was calculated using the formula (1). The time evolution of E_{HA} shows that the duration of the EMP exhibiting only a few oscillations is shorter than 3 ns and the corresponding decay time τ_{dec} is of the order of a nanosecond. While $E_{HA}(t)$ reaches 46% of its maximum value in ≈ 3 ns, $E_{RS}(t)$ reaches it in just 0.5 ns. Figure 6c shows an example of the STFT (Short-Time Fourier Transform) of S_{HA} detected at shot 61812, where the dominant frequency f_c ≈ 1.1 GHz. This also shows that the EMP reaches its peak about 1 ns after the arrival of the maximum laser intensity. The frequency spectrum presented in Figure 6d reveals the dominant frequency lying in the range 0.8-1.5 GHz band. Frequencies from the 1.5 - 2.2 GHz band occur only in some shots.

Figure 6 EMP induced by a single 350-ps, 125-J laser pulse.

The HA signals proved that the occurrence of a laser spark is accompanied by the EMP pulse. This microwave EMP is caused by time-varying currents originating from various sources such as ions, runaway electrons, and slow electrons. The runaway (hot) electrons from the laser kernel into the surrounding cold gas, where they produce secondary electrons in collisions with gas molecules. The runaway electrons thus cause the formation of an electrical double layer at the interface between the laser kernel and the surrounding gas, where the positive charge is located on the surface of the laser kernel and the negative charge is in the layer of gas touching the kernel. From a phenomenological point of view, the double layer can be considered a potential well. The positive charge of this potential well is created by the escape of hot electrons from the laser kernel, while the negative charge is created by these runaway electrons being captured by the cold gas near the core. Thus, the boundary between the kernel and the cold gas could be termed as a spark double layer (SDL). S. Eliezer and H. Hora approximated the hydrodynamic bounce frequency, ω_{PW}, in such a potential well by the relationship [43]:

$$\omega_{PW} = \frac{2\pi}{l}\sqrt{\frac{e\phi_0}{m}}, \tag{5}$$

where l is the dimension of the potential well, i.e. the SDL thickness comparable to the mean free path of electrons, ϕ_0 is the SDL potential, and m is the electron mass. The electric field could be found by solving Poisson's equation for the electrostatic potential in combination with equations for the density of low-energy electrons, positive and negative ions including the runaway electron mechanism. Please note that the temporary experimental technique does not allow us to measure this potential.

https://doi.org/10.1017/hpl.2025.10061 Published online by Cambridge University Press

It is reasonable that the knowledge of the different periods of the EMP (frequency spectrum) and corresponding decay times on a short time scale can provide basic experimental information about the mechanism of ion production in the vicinity of the spark kernel. We note that no natural frequencies or resonant modes affected the frequency spectrum of the EMP emitted by the laser-produced spark in the gas.

The mechanism of runaway electrons in a laser spark is fundamentally different from the mechanism of runaway electrons that are produced when a laser pulse interacts with a solid target placed in the vacuum. First, many orders of magnitude more electrons are generated during solid target ablation than in laser spark mode. Second, the electron flux escaping from the spark is therefore many times smaller and is stopped by collisions with particles of the surrounding gas, while in the case of solid targets irradiated in a vacuum, the runaway electrons pass a long way to the walls of the vacuum chamber. Therefore, the intensity of the EMP generated in a laser spark discharge is less than in the case of solid targets irradiated in a vacuum, as shown in Figure 7. The presented comparison shows that the energy absorbed by HA was about 4000 times higher by detecting the EMP emitted by the interaction of the laser with the copper target than by the spark produced in SF_6 by a laser delivering the same energy. However, in this case, the HA detected the EMP from the Cu plasma at 4.5 m from the target, while in the experiment with SF_6 it was located only 2.5 m from the spark. We can conclude that the EMP gain from a laser spark is a thousand times smaller than when the laser interacts with solid particles placed in vacuum.

Figure 7 Comparison of energy absorbed by HA

Although the mechanism of broadband emission from a laser spark is not yet fully understood, there is some similarity in the EMP spectra, both when using ultrafast laser pulses and nanosecond pulses. It turns out that an important parameter is pressure, expressed, for example, in the density of the irradiated gas. At the same or higher density of gas irradiated with 30 fs laser pulses, the frequency spectra had a range of around 0.8 - 2 GHz [44], as in our experiment. On the contrary, with decreasing gas pressure, not only does the amplitude of the electromagnetic field increase, and frequencies higher than the 3 GHz registered by us are also generated, as shown by the experiment of A. Engelsbe et al. [45]. At a pressure of 66 Pa, the 50fs laser generated approximately a hundred times more intense EMP than at a pressure of 84 kPa. However, 10 GHz and higher frequency were well pronounced. In the case of PALS

https://doi.org/10.1017/hpl.2025.10061 Published online by Cambridge University Press

experiments with solid targets, frequencies higher than 3 GHz are also generated [46]. These experimental results support our idea that SDL could be a source of EMP.

3.3. Laser spark visualisation

A photograph of a glowing spark can provide a basic insight into the plasma distribution in the cell, as shown in Figure 8. Please note that this is a time-integrated image of transient laser spark emission taken in the visible spectrum. The laser pulse arrives from the right after passing through a lens with a focal length of 300 mm and then an input cell window. Luminescence of the laser-irradiated SF_6 occurs as soon as the laser pulse enters the cell, where it reaches an intensity of about 5×10^9 W/cm^2. As the image shows, the luminescence appears on microislands that are irregularly distributed in the cell. The life cycle of a spark can reach up to tens of microseconds [47, 48].

Figure 8 Passive laser spark imaging

Figure 8 shows that the spark length is ~4.3 cm. This dimension can be considered the limiting dimension of a spark emitting visible radiation. However, the dimensions of the kernel with the released electrons will probably be smaller. Regardless of the mechanism of the magnetic field generation in the kernel that affects the trajectories of the boundary secondary electrons, it is evident that the number of these boundary electrons is very small. Assuming that the signal of the magnetic probe localized in the near zone is induced only by the electron current flowing through the laser spark, a rough estimate of the peak current value indicates a current of only up to 100 mA. It corresponds to a current only of about 10^8 electrons. Please note that the first estimate of the magnetic and electric field intensities did not consider the possibility of laser spark generation in an electronegative gas [41].

The laser creates a kernel consisting of fully ionized fluorine and almost fully ionized sulphur as well as electrons. Please note that although we did not measure the mass spectra of the kernel-forming ions, we can estimate the degree of ionization of the S and F elements from the spectra of polytetrafluoroethylene (PTFE) ionized with an equivalent laser energy of ~150 J also delivered by the PALS beam, which identified F^{9+} ions far from the target [49]. The kernel formed by multiply ionized S and F ions expands into the background gas, creating a "bubble" around the focus. In addition, this kernel is a source of UV and X-ray radiation, which are absorbed by SF_6. This produces a secondary plasma core within SF_6, in which the separation of electrons and ions also occurs.

https://doi.org/10.1017/hpl.2025.10061 Published online by Cambridge University Press

3.4. Single shot optical emission spectra

To help characterize a laser spark, a fibre optic spectrometer is used to analyze the emissions from the spark. The recorded spectra contain both the continuum background originating from the hot plasma kernel and the visible spectrum of recombining ions and excited atoms during laser spark quenching, as Figure 9 shows. This spectrum has a similar profile to the spectra of laser-generated sonoluminescent bubbles, which exhibit the characteristic blackbody spectrum (background continuum) observed in both laser-produced and high-voltage discharge plasmas [50 - 52]. The observed emission spectra are affected by the dramatically changing temperature determining blackbody radiation that occurs during the early phase of spark production. For these reasons, it was not possible to perform the best fit of the continuum background using the Planck law function of blackbody radiation. Although the background spectrum has been reported in several papers, its nature is still unclear. Therefore, we simulated the background signal using three bigaussian functions with central wavelengths of 412.7, 500.7 and 561.2 nm.

Figure 9 Optical emission spectra of high-power-laser sparks produced in SF_6.

The presented spectroscopic lines data of sulphur and fluorine are from the National Institute of Standards and Technology (NIST) atomic spectra database [53]. These were superimposed on the background signal so that the resulting spectrum matched the observed spectrum. Due to the varying temperature, T_e, and density, n_e, of electrons during spectrum recording, no average values of these parameters were used to exactly specify spectral peaks of S and F ions and atoms. However, the spectrum was divided into three wavelength ranges of 300–460, 460–600, and 600–720 nm to help clarify the origin of the spectral lines. In the first wavelength range of 300 - 400 nm, the S III spectral lines dominate, which approximately correspond to T_e=2.2 eV and n_e=1×10^{17} cm^{-3}. The decisive parameter is the electron temperature. When T_e drops to about 1 eV, lines from the second range appear, which

https://doi.org/10.1017/hpl.2025.10061 Published online by Cambridge University Press

correspond mainly to S II lines. The fluorine lines F I dominate for T_e = 0.9 eV and n_e=1×10^{14} cm^{-3} in the third range of 600 – 720 nm. Although we did not measure optical emission spectra (OES) as a function of time and, thus, did not obtain time-resolved values of T_e and n_e, the values estimated in our experiment are like those obtained in the experiment with a laser spark produced in air with a very low pulse energy of 40-150 mJ performed by Ş. Yalçin et al. [54]. $T_e \approx$ 1 eV obtained by Yalçin et al. were detected more than 1 μs after the end of the laser interaction. However, T_e in the kernel should reach much higher values (hundreds of eV). T_e estimated from optical emission spectra of plasmas produced in SF_6 gas-puff target by a focused beam of the neodymium laser delivering 15J of energy in 1 ns [55].

Although the purity of the SF_6 used was 99.9%, the impurity content of 0.1% in the gas and impurities absorbed on the inner surface of the cell allowed detection of the H_α line with a wavelength of 656.28 nm, as Figure 10 shows. Due to the low impurity content, the amplitude of the H_α line is small. However, the estimation of the H_α line width is crucial because it is assumed to be reciprocally correlated with the electron density of the plasma due to the Stark broadening [54, 56 - 58].

Figure 10 Detail of optical emission spectra of laser sparks produced in SF_6 at 101.3 kPa.

Stark broadening can lead to asymmetric line profiles, which can be analyzed by fitting a Voigt function to the observed H_α line profile to determine the full width at half maximum, w_{FWHM}, of the spectral line. Using this technique, which is widely used in various types of plasmas, the magnitude of the electron density, n_e, can be calculated using the relationship [57]:

$$n_e = \left(\frac{w_{FWHM}}{1.098}\right)^{1.4713} \times 10^{17}\ cm^{-3}. \quad (5)$$

Using the relationship (5) we obtain $n_e \sim 10^{17}$ cm^{-3}. This value correlates with the estimated value for the S III wavelength range shown in Figure 10.

https://doi.org/10.1017/hpl.2025.10061 Published online by Cambridge University Press

The contribution of the Gaussian profile width to the total line is comparable to the Lorentzian width for other spectral lines, e.g. the S V triplet at 703 nm. This triplet S V and the

Figure 11 Detail of optical emission spectra of laser sparks produced in SF_6 at 26.7 kPa.

3 fitted Voigt functions are shown in Figure 11. Fitting gave $w_G = 0.146$ and $w_L = 0.337$ being shared for all functions. The S V triplet was analysed using the Voigt function with the PeakFit software.

3.5. Shot-to-shot reproducibility

Like other experiments dedicated to the interactions of high-power laser pulses with solids, the presented experiment exhibits significant shot-to-shot fluctuations. Fluctuations relate not only to the emission of electrons, ions and possibly products of fusion processes, but also to the emission of EMP and the continuum background. The range of EMP fluctuations during the interaction of a ~370 GW laser pulse with gas is shown in Figure 12.

Figure 12 Time course of the energy of the horn antenna signal.

The time-resolved dependence of the energy absorbed by the horn antenna shows that fluctuations occur already during the first phase of the laser-SF_6 interaction, i.e. during the first 200 ps. The energy absorbed by the horn antenna fluctuates from 0.25 - 1.8 nJ in this period, while the fluctuations of the delivered laser energy are $< \pm 5\%$. The efficiency of converting laser energy into EMP energy, which is related to the flow of electrons escaping from the spark kernel, therefore indicates significant fluctuations in the absorption of laser radiation by the gas, like the case of laser-solid interaction. However, please note that there is a significant difference between the two interactions, namely that the electron concentration, n_e, in the case of SF_6 cannot reach values higher or equal to the critical value, n_c. However, in the case of fully stripped F and S atoms, the electron density can reach values higher than $n_c/4$, and the

https://doi.org/10.1017/hpl.2025.10061 Published online by Cambridge University Press

absorption of laser radiation can be affected by the instability of two-plasmon decay (TPD) [13, 59].

Shot-to-shot fluctuations also occur in emission of visible light, as Figure 13 shows. The curves show the average intensity recorded by the camera during 3 series of shots. Fresh SF_6 charge was used in the first and second series, while the charge from the second series was used in the third series, but the break between them was 19 hours (the average is shown by the red line labelled as "1st shots"). The luminosity of the first shots fluctuated around 5% percent. It always dropped by 20% percent with the second shot (see the black line "subsequent shots"). Starting with the second shot, the luminosity fluctuated within ±10%. The subsequent shots were repeated with a period of ~30 minutes.

Figure 13 Intensity profile along the caustic line evaluated from spark photographs.

The shot-to-shot fluctuations in spark luminosity are different from fluctuations in EMP emission and continuum background. While fluctuations in the luminosity of the sparks produced by the second and subsequent shots are steadily at the level of 10%, the EMP fluctuations are more pronounced, as shown in Figure 12. However, both phenomena, emission of EMP and visible radiation, are detected at different stages of spark production and extinction and are therefore driven by different mechanisms.

3.6. Chemical change initiated by laser spark

From a chemical point of view, the interaction experiments reported here can be divided into two groups. In the first one, gaseous SF_6 contained naturally admixed moist air ($N_2/O_2/CO_2/H_2O$) so that the conditions corresponded to those that can be expected in the normal use of SF_6 as an industrial gaseous dielectric. In the second series of experiments, SF_6 contained admixtures of dry air only ($N_2/O_2/CO_2$). A moisture (H_2O) was excluded from all

https://doi.org/10.1017/hpl.2025.10061 Published online by Cambridge University Press

gases as well as gas handling systems and procedures used. Final products formed in reactions initiated by PALS-produced plasmas have been in both series analysed using the gas chromatography with mass spectrometry detection (GC-MS).

In samples containing the moist air, gas chromatograms reveal only three products of SF_6 reactions, i.e., thionyl fluoride (SOF_2), sulfuryl fluoride (SO_2F_2) and thionyl tetrafluoride (SOF_4). Yields of all three products are low (~1%). Their abundances depend on a pressure in the cell. At $p(SF_6)$ = 10.7 kPa, i.e., the lowest pressure in the cell, there are SOF_2 and SOF_4 formed (Figure 14). If we increase the pressure of SF_6 to 26.7 kPa, SOF_2 and SO_2F_2 appear as products. At even higher SF_6 pressures, i.e., 53.3 kPa and 101.3 kPa (atmospheric pressure), only one product (SOF_2) is indicated. The overall (stoichiometric) reactions leading to the above-mentioned final products could be expressed in the way as follows:

$$SF_6 + H_2O \rightarrow SOF_2 + 2HF + F_2$$

$$SF_6 + 2H_2O \rightarrow SO_2F_2 + 4HF$$

$$SF_6 + H_2O \rightarrow SOF_4 + 2HF$$

However, neither HF/ F_2 nor SiF_4 molecules have been indicated in GC records. The silicon tetrafluoride should be formed in reactions of hydrogen fluoride and/or molecular fluorine with SiO_2 in the cell wall.

Figure 14 The gas chromatogram of SF_6 chemically altered by LIDB plasmas

Contrary to the samples contaminated by moist air, the samples that do not contain traces of water vapour exhibit quite poor laser-plasma chemical reactivity. In addition to remaining SF_6 and air, only sulfuryl fluoride (SO_2F_2) has been found in the gas cell after 4 and 8 laser shots accumulated at initial total pressures varied from 10.7 kPa to 101.3 kPa. Therefore, SO_2F_2 molecules represent a single stable product which testifies to the key role of molecular oxygen (and transient species formed from its molecule upon LIDB conditions) in the reaction mixture because water vapour is not present in these runs. Considering the situation just

https://doi.org/10.1017/hpl.2025.10061 Published online by Cambridge University Press

stoichiometrically, the overall reaction $SF_6 + O_2 \rightarrow SO_2F_2 + 2F_2$ provides sulfuryl fluoride. However, the reaction gives molecular fluorine as another product which has not been registered by GC-MS.

Notable is the absence of SiF_4, which is thought to be formed by reactions of fluorine, hydrogen fluoride and other fluorine containing reactive species with SiO_2 in the glass body of the cell and its window. The SiF_4 formation was observed in a narrow (1.44 cm in dimeter) cell filled with SF_6 in which the focused TEA CO_2 laser produced LIDB plasmas [60]. In the experiment reported here, much larger inner diameter of the cell and the use of a long focal length lens ensure that fluorine reactants do not penetrate a mass of ambient, unirradiated gas towards the cell wall and the beam entrance window. Therefore, silicon tetrafluoride is not formed under these conditions. Both larger dimensions of the cell and strong reduction of gas mixture contact with carbon containing components (e.g., o-rings, vacuum grease, and flanges made of plastics) and contaminants (hydrocarbons from vacuum line) are likely responsible for an absence of CF_4 formation. This product has also been frequently reported in SF_6 subjected to electrical discharges [61] and laser sparks [60], when fluorine-rich products and transients interact with carbon containing species and surfaces in the gas cell.

In conclusion, we can say that the fully reproducible chemical change can be registered and quantified under irradiation conditions applied here. Conversion efficiency and formation yields of the initial substance (SF_6) and final products (SO_xF_y), respectively, are both low. In addition to that, number of products is very low, i.e., only one-two products depending on water vapour content and a pressure of the initial substance. The absence of any S_xF_y molecule (e.g., SF_4 and/or S_2F_{10}) among products leads to the assumption that product forming reactions here are not stepwise unimolecular decompositions starting from SF_6 [61-65], but rather bimolecular reactions of the initial substance with oxygen species (e.g., molecular, and atomic oxygen, hydroxyl radical, and water molecules). All the above-mentioned findings contrast with those

https://doi.org/10.1017/hpl.2025.10061 Published online by Cambridge University Press

(especially a wide variety of products) obtained in electrical discharges between electrodes (see for example [61, 14] and references cited therein), conventional pyrolysis in a resistively heated reaction tube [66], and lasers sparks induced in a narrow gas cell [60, 67], where an interaction of plasmas (including radiation, particles and reactive species liberated from the plasma [14,60,61,65] or hot gas [66] with solid surfaces can take place. Under our experimental conditions, an influence of solid surfaces on plasma-chemical SF_6 decomposition patterns seems to be significantly reduced.

4. CONCLUSIONS

SF_6 plasma produced by a 350-ps, 126-J near-infrared laser pulse is a complex object with parameters evolving on different time scales. After the energy deposition, spontaneous relaxation of the laser spark occurs, releasing excess energy. During the interaction of the laser pulse with the gas, there is not only fragmentation and ionization of SF_6, but also escape of hot electrons from the plasma kernel, which produce spontaneous magnetic field and emit EMP. The EMP emission from a laser spark is very weak compared to the EMP produced when such a laser pulse interacts with a solid target placed in vacuum. This is due to the loss of energy of runaway electrons in collisions with molecules of the surrounding cold gas. The frequency of about 1.1 GHz is a typical frequency of EMP emitted from the SF_6 laser spark at atmospheric and sub-atmospheric pressures. The frequency spectrum of the spontaneous magnetic field is broader and contains three bands around 1.15, 2.1 and 3 GHz. These fields cease within 5 ns.

After being heated by the laser, the plasma undergoes a relaxation process that can last up to microseconds, during which charged particles recombine, ions and atoms emit radiation in the visible part of the spectrum. Although the evolution dynamics in recombining SF_6 plasma was not measured using a time-resolved spectrometer, it was estimated that the values of n_e and

https://doi.org/10.1017/hpl.2025.10061 Published online by Cambridge University Press

T_e do not differ from those experimentally observed, e.g., in the field of Laser-Induced Breakdown Spectroscopy (LIBS).

The primary motivation for the fabrication and engagement of the gas cell with relatively large diameter was to eliminate the effects of the walls, flanges, and beam entrance window on the plasma processes responsible for EMP generation. However, this specific feature of the cell design was also influencing the chemical change in SF_6 registered under these experimental conditions. Gas chromatography showed the formation of only a very limited number of products and a low degree of conversion of SF_6. This contrasts with results obtained by other researchers [14,60-67] in electrical discharges, electrically heated tube reactors for pyrolysis or also with laser sparks, but in small gas cells, where solids can influence SF_6 decomposition mechanisms and rates, often dramatically. Under experimental conditions described here, the laser-plasma-chemical reaction system proved to be perfectly homogeneous. A detailed report on laser-plasma chemical results and their mechanistic implications (what specific physical and chemical processes are responsible for a particular chemical change; the methodology can be found in refs [68, 69]) is being prepared to appear in a chemical journal.

The shot-to-shot fluctuations in emission of EMP and visible radiation reflect two fundamental stages occurring during the lifetime of the laser spark. The first is plasma producing by a laser pulse, where competing picosecond processes control the energy of electrons and their flows generating spontaneous magnetic field and EMP. This phase is characterized by significant fluctuations in the magnetic field intensity and the background continuum of the visible radiation. The second phase begins after laser heating of SF_6. The processes of plasma recombination and chemical reactions leading to the formation of SF_6, F_2, SF_4 and various sulphur oxyfluorides occurring on a microsecond scale are accompanied by fluctuations in the emission of visible radiation, which, however, are much smaller compared to the fluctuations mentioned above.

https://doi.org/10.1017/hpl.2025.10061 Published online by Cambridge University Press

ACKNOWLEDGEMENT

Authors' thanks go to the Czech Ministry of Education, Youth and Sports (CMEYS) for the financial support of the project nr. LM2023068 (PALS RI) and to the Grant Agency of the Czech Republic (Project No. GM23-05027M).

References

1. H. Moissan and P. C. R. Lebeau, "Sur un nouveau corps gazeux: Le perfluorure de soufre SF_6", Acad. Sci. Paris Compt. Rrend. 130, 865-871 (1900).
2. L. G. Christophorou and J. K. Olthoff, "Electron interactions with SF_6", J. Phys. Chem. Ref. Data 29, 267-330 (2000). DOI: https://doi.org/10.1063/1.1288407
3. V. N. Maller and M. S. Naidu, *High Voltage Insulation and Arc Interruption in SF_6 and Vacuum*, (Pergamon Press, Oxford-NY-Toronto-Sydney-Paris-Frankfurt 1981).
4. F. Y. Chu, "SF_6 decomposition in gas-insulated equipment", IEEE Trans. Electr. Insul. EI-21, 693-725 (1986). DOI: https://doi.org/10.1109/TEI.1986.348921
5. W.-T. Tsai, "The decomposition products of sulfur hexafluoride (SF_6): Reviews of environmental and health risk analysis", J. Fluor Chem. 128, 1345–1352 (2007). DOI: https://doi.org/10.1016/j.rser.2021.110759
6. D. Rombach and H.-A. Wagenknecht, "Photochemical activation of sulfur hexafluoride: A tool for fluorination and pentafluorosulfanylation reactions", *Synthesis* 54, 4883–4894, (2022). DOI: 10.1055/a-1877-5231.
7. G. Brederlow, E. Fill, and K. J. Witte, *The High-Power Iodine Laser*, Springer-Verlag, Berlin-Heidelberg 1983.
8. L. Láska, J. Krása and L. Juha, "Chemistry of iodine photodissociation lasers at the pyrolytic regime", Chem. Phys. 172, 377-385 (1993). DOI:10.1016/0301-0104(93)80131-r.
9. V. M. Orlovski, E. A. Sosnin, V. F. Tarasenko, A. G. Ponomarenko and Yu. I. Khapov, "Efficiency of an electron-beam-pumped chemical laser with an SF_6-H_2 working mixture", Tech. Phys. 44, 69-73 (1999). DOI: https://doi.org/10.1134/1.1259254
10. D. M. Manos, D. L. Flamm, *Plasma Etching: An Introduction*, (Academic Press, Boston 1989).

11. T. Kampfrath, L. Perfetti, D. O. Gericke, C. Frischkorn, P. Tegeder and M. Wolf, "Ultrafast capture of free electrons in optically ionized gases by the electron scavenger SF_6", Chem. Phys. Lett. 429, 350-354 (2006). https://doi.org/10.1016/j.cplett.2006.08.038
12. S. Tian, X. Zhang, Y. Cressault, J. Hu, B. Wang, S. Xiao, Y. Li, and N. Kabbaj, "Research status of replacement gases for SF_6 in power industry", AIP Advances 10, 050702 (2020). DOI: https://doi.org/10.1063/1.5134727
13. W. Seka, J. F. Myatt, R.W. Short, D. H. Froula, J. Katz, V. N. Goncharov, and I. V. Igumenshchev, "Nonuniformly driven two-plasmon-decay instability in direct-drive implosions", Phys. Rev. Lett. 112, 145001 (2014). DOI: https://doi.org/10.1103/PhysRevLett.112.145001
14. R. Kurte, H. M. Heise, and D. Klockow, "Quantitative infrared spectroscopic analysis of SF_6 decomposition products obtained by electrical partial discharges and sparks using PLS-calibrations", J. Mol. Struct. 565-566, 505-513 (2001). DOI:https://doi.org/10.1016/S0022-2860(00)00847-4
15. F. Consoli, V. T. Tikhonchuk, M. Bardon, P. Bradford, D. C. Carroll, J. Cikhardt, M. Cipriani, R. J. Clarke , T. E. Cowan, C. N. Danson, R. De Angelis, M. De Marco, J.-L. Dubois , B. Etchessahar, A. L. Garcia, D. I. Hillier, A. Honsa, W. Jiang, V. Kmetik, J. Krása, Y. Li, F.Lubrano, P. McKenna, J. Metzkes-Ng, A. Poyé, I. Prencipe, P. Raczka, R. A. Smith, R. Vrana, N. C. Woolsey, E. Zemaityte, Y. Zhang, Z. Zhang, B. Zielbauer, and D. Neely, "Laser produced electromagnetic pulses: Generation, detection and mitigation", High Power Laser Sci. Eng. 8, E22 (2020). DOI: https://doi.org/10.1017/hpl.2020.13
16. C. G. Brown Jr., J. Ayers, B. Felker, W. Ferguson, J. P. Holder, S. R. Nagel, K. W. Piston, N. Simanovskaia, A. L. Throop, M. Chung, and T. Hilsabeck. "Assessment and mitigation of diagnostic-generated electromagnetic interference at the National Ignition Facility". Rev. Sci. Instrum. 83, 10D729 (2012). DOI: https://doi.org/10.1063/1.4739313
17. P. Bradford, N. C. Woolsey, G. G. Scott, G. Liao, H. Liu, Y. Zhang, B. Zhu, C. Armstrong, S. Astbury, C. Brenner, P. Brummitt, F. Consoli, I. East, R. Gray, D. Haddock, P. Huggard, P. J. R. Jones, E. Montgomery, I. Musgrave, P. Oliveira, D. R. Rusby, C. Spindloe, B. Summers, E. Zemaityte, Z. Zhang, Y. Li, P. McKenna, and D. Neely. "EMP control and characterization on high-power laser systems". High Power Laser Sci. Eng. 6, e21 (2018). DOI: https://doi.org/10.1017/hpl.2018.21

https://doi.org/10.1017/hpl.2025.10061 Published online by Cambridge University Press

18. G. Dahlbacka, J. Guillory. “Laser induced EMP (electromagnetic pulse) at 10.6 microns”, *NASA STI/Recon Technical Report N*, 1987, 87: 29819.
19. J.-L. Dubois, F. Lubrano-Lavaderci, D. Raffestin, J. Ribolzi, J. Gazave, A. Compant La Fontaine, E. d’Humieres, S. Hulin, Ph. Nicolaï, A. Poyé, and V. T. Tikhonchuk, “Target charging in short-pulse-laser–plasma experiments”, Physical Review E 89, 013102 (2014)
20. A. Poyé, S. Hulin, M. Bailly-Grandvaux, J. Ribolzi, D. Raffestin, M. Bardon, F. Lubrano-Lavaderci, J. J. Santos, P. Nicolaï, and V. Tikhonchuk, “Physics of giant electromagnetic pulse generation in short-pulse laser experiments”. Phys. Rev. E 91, 043106 (2015). DOI:https://journals.aps.org/pre/abstract/10.1103/PhysRevE.97.019903
21. J. Cikhardt, J. Krása, M. De Marco, M. Pfeifer, A. Velyhan, E. Krouský, B. Cikhardtová, D. Klír, K. Řezáč, J. Ullschmied, J. Skála, P. Kubeš, and J. Kravárik, “Measurement of the target current by inductive probe during laser interaction on terawatt laser system PALS”, Review of Scientific Instruments 85, 103507 (2014)
22. M. J. Mead, D. Neely, J. Gauoin, R. Heathcote, and P. Patel, “Electromagnetic pulse generation within a petawatt laser target chambre”, Rev. Sci. Instrum. 75, 4225 (2004). DOI: http://dx.doi.org/10.1063/1.1787606
23. S. Herzer, A. Woldegeorgis, J. Polz, A. Reinhard, M. Almassarani, B. Beleites, F. Ronneberger, R. Grosse, G. G. Paulus, U. Hübner, T. May and A. Gopal. “An investigation on THz yield from laser-produced solid density plasmas at relativistic laser intensities”, New J. Phys. 20, 063019 (2018). DOI:https://doi.org/10.1088/1367-2630/aaada0
24. G. Liao, Y. Li, H. Liu, G. G. Scott, D. Neely, Y. Zhang, B. Zhu, Z. Zhang, C. Armstrong, E. Zemaityte, P. Bradford, P. G. Huggard, D. R. Rusby, P. McKenna, C. M. Brenner, N. C. Woolsey, W. Wang, Z. Sheng, and J. Zhang. “Multimillijoule coherent terahertz bursts from picosecond laser-irradiated metal foils”. Proc. Natl. Acad. Sci. 116, 3994-3999 (2019). DOI: https://doi.org/10.1073/pnas.1815256116
25. I. Thiele, R. Nuter, B. Bousquet, V. Tikhonchuk, and S. Skupin. “Theory of terahertz emission from femtosecond-laser-induced microplasmas”. Phys. Rev. E 94, 063202 (2016). https://doi.org/10.1103/PhysRevE.94.063202
26. A. Englesbe, J. Elle, R. Schwartz, T. Garrett, D. Woodbury, D. Jang, Ki-Yong Kim, H. Milchberg, R. Reid, A. Lucero, D. Gordon, R. Phillips, S. Kalmykov, and A. Schmitt-Sody. “Ultrabroadband microwave radiation from near- and mid-infrared laser-

https://doi.org/10.1017/hpl.2025.10061 Published online by Cambridge University Press

produced plasmas in air". Phys. Rev. A 104 013107 (2021). DOI:https://doi.org/10.1103/PhysRevA.104.013107

27. C. L. Longmire, "On the electromagnetic pulse produced by nuclear explosions", IEEE Trans. Electromagnetic Compatibility, 20, 3-13(1978). https://doi.org/10.1109/TEMC.1978.303688 .
28. Y. Cui, J. Jiang, D. Kong."Characteristics and variation laws of electromagnetic radiation generated during explosion". Prop. Explos. Pyrotech. 49, e202300166 (2024). DOI:https://doi.org/10.1002/prep.202300166
29. A. J. Reid and M. D. Judd, "Ultra-wide bandwidth measurement of partial discharge current pulses in SF_6", J. Phys. D: Appl. Phys. 45, 165203 (2012). http://dx.doi.org/10.1088/0022-3727/45/16/165203
30. G. C. Stone, A. Cavallini, G. Behrmann, C. A. Serafino, *Practical Partial Discharge Measurement on Electrical Equipment* (John Wiley& Sons: Hoboken, NJ, USA, 2023), p. 137.
31. S. A. Boggs and G. C. Stone. "Fundamental limitation in the measurement of corona and partial discharge", IEEE Trans. Electrical Insulation EI-17, 143-150 (1982). https://doi.org/10.1109/TEI.1982.298548
32. X.-L. Liu, X. Lu, J.-L. Ma, L.-B. Feng, X.-L. Ge, Y. Zheng, Y.-T. Li, L.M. Chen, Q.-L. Dong, WM. Wang, Z.-H. Wang, H. Teng, Z.-Y. Wei, J. Zhang. "Long lifetime air plasma channel generated by femtosecond laser pulse sequence". Opt. Express 20, 5968-5973 (2012). DOI:https://doi.org/10.1364/OE.20.005968
33. S. S. Harilal, P. J. Skrodzki, A. Miloshevsky, B. E. Brumfield, M. C. Phillips, G. Miloshevsky. "On- and off-axis spectral emission features from laser-produced gas breakdown plasmas", Phys. Plasmas 24, 063304 (2017). http://dx.doi.org/10.1063/1.4985678
34. A. V. Mitrofanov, A. A. Voronin, M. V. Rozhko, D. A. Sidorov-Biryukov, M. M. Nazarov, A. B. Fedotov, A. M. Zheltikov. "Polarization and spatial mode structure of mid-infrared-driven terahertz-to-microwave radiation", ACS Photonics 8, 1988−1996 (2021). DOI:https://doi.org/10.1021/acsphotonics.0c01966
35. A. Bartnik, W. Skrzeczanowski, J. Czwartos, J. Kostecki, H. Fiedorowicz, P. Wachulak, T. Fok, „Low temperature plasmas induced in SF_6 by extreme ultraviolet (EUV) pulses". Phys. Plasmas. 25, 063508 (2018). https://doi.org/10.1063/1.5030965
36. N. Guthikonda, D. P. S. L. Kameswari1, E. Manikanta, S. Sai Shiva, S. Sree Harsha, V. R. Ikkurthi, P. Prem Kiran. "Dynamics of spatially confined ns laser induced

https://doi.org/10.1017/hpl.2025.10061 Published online by Cambridge University Press

atmospheric air plasma and shock waves: visualization vis-à-vis validation". J. Phys. D: Appl. Phys. 56, 305501, (2023). DOI: https://doi.org/10.1088/1361-6463/accf25

37. K. Jungwirth, A. Cejnarová, L. Juha, B. Králiková, J. Krása, E. Krouský, P. Krupičková, L. Láska, K. Mašek, T. Mocek, M. Pfeifer, A. Präg, O. Renner, K. Rohlena, B. Rus, J. Skála, P. Straka, J. Ullschmied, "The Prague Asterix Laser System", Phys. Plasmas **8**, 2495 (2001). DOI: https://doi.org/10.1063/1.1350569
38. J. A. Stamper, "Review on spontaneous magnetic fields in laser-produced plasmas: Phenomena and measurements", Laser Part. Beams 9, 841–862 (1991). DOI: https://doi.org/10.1017/S0263034600006595
39. V. V. Korobkin, R.V. Serov "Investigation of the magnetic field of a spark produced by focusing laser radiation", JETP Lett. 4, 70 (1966).
40. Yu. P. Raizer, "Lazernaya iskra i rasprostranenie razriadov" (Moskva: Izdatelstvo Nauka 1974); see also Raizer, Yu. P, *Laser-induced discharge phenomena* (New York, London: Consultants Bureau,1977).
41. K. Rohlena, and M. Mašek, "Ambient fields generated by a laser spark", Nukleonika, 61, 119-124 (2016). DOI:http://www.nukleonika.pl/www/back/full/vol61_2016/v61n2p119f.pdf
42. rohde-schwarz.com
43. S. Eliezer and H. Hora, "Dynamic electric fields and double layers in laser-produced plasmas", Fusion Technology 16, 419-463 (1989). DOI: https://doi.org/10.13182/FST89-A29107
44. Q.-Y. He, Z.-T. Wang, ·Z.-G. Deng, J. Feng. Y.-D. Xia, X.-C. Hu, M.-Y. Zhu, J.-J. Xie, Z.-Q. Yuan, Z.-M. Zhang, F. Lu, L. Yang, H. Cheng, Y.-Z. Li, Y. Yan, Y.-L. Fang, C.-T. Li, W.-M. Zhou, T.-S. Li, L.-M. Chen, Ch. Lin, X.-Q. Yan, "Generation and regulation of electromagnetic pulses induced by multi-petawatt laser coupling with gas jets". Nuclear Science and Techniques (2025) 36:100. DOI: https://doi.org/10.1007/s41365-025-01692-6
45. A. Englesbe, J. Elle, R. Reid, A. Lucero, H. Pohle, M. Domonkos, S. Kalmykov, K. Krushelnick, A. Schmitt-Sody, "Gas pressure dependence of microwave pulses generated by laser-produced filament plasmas". Optics Letters. 43, 4953-6 (2018). DOI DOI https://doi.org/10.1364/OL.43.004953
46. J. Cikhardt, P. W. Bradford, M. Ehret, S. Agarwal, M. Alonzo, P. Andreoli, M. Cervenak, V. Ciardiello, F. Consoli, D. Davino, J. Dostal, R. Dudzak, D. Klir, J. Krasa, M. Krupka, P. Kubes, J. Malir, C. Mendez, V. Munzar, J. Novotny, O. Renner, K.

https://doi.org/10.1017/hpl.2025.10061 Published online by Cambridge University Press

Rezac, M. O. Ruiz, J. J. Santos, M. Sciscio, S. Singh, Z. Valdova, L. Juha, M. Krus, "Comprehensive characterization of electromagnetic pulses driven by sub-nanosecond kilojoule laser" *High Power Laser Science and Engineering* (2025) accepted. DOI: 10.1017/hpl.2025.10035.

47. S. S. Harilal, B. E. Brumfield, M. C. Phillips. “Lifecycle of laser-produced air sparks”. Phys. Plasmas 22, 063301 (2015). DOI:http://dx.doi.org/10.1063/1.4922076
48. H. Sun, H. Chang, M. Rong, Y. Wu, H. Zhang. “Investigation of laser-induced plasma in SF_6 at different pressures using Thomson scattering”. Phys. Plasmas 27, 073508 (2020). DOI:https://doi.org/10.1063/5.0009906
49. J. Krása, A. Velyhan, K. Jungwirth, E. Krouský, L. Láska, K. Rohlena, M. Pfeifer, J. Ullschmied. “Repetitive outbursts of fast carbon and fluorine ions from sub-nanosecond laser-produced plasma”, Laser Part. Beams 27, 171–178 (2009). DOI:https://doi.org/10.1017/S0263034609000238
50. B. Kappus, S. Khalid, A. Chakravarty, and S. Putterman. “Phase transition to an opaque plasma in a sonoluminescing bubble”. Phys. Rev. Lett. 106, 234302 (2011). http://dx.doi.org/10.1103/PhysRevLett.106.234302
51. T. Sato, M. Tinguely, M. Oizumi, M. Farhat, “Evidence for hydrogen generation in laser-or spark-induced cavitation bubbles”, Appl. Phys. Lett. 102, 074105 (2013). DOI: http://dx.doi.org/10.1063/1.4793193
52. J. T. Krile, R. Vela, A. A. Neuber, H. G. Krompholz, “Spectral analysis of pulsed volume breakdown in SF_6 at high pressures”, IEEE Trans. Plasma Sci. 35, 1163-1169 (2007). DOI:https://doi.org/10.1109/TPS.2007.902014
53. A. Kramida, Y. Ralchenko, J. Reader, NIST ASD Team National Institute of Standards and Technology NIST. “Atomic Spectra Database”, Available online: http://physics.nist.gov/asd (accessed on 9 January 2025).
54. Ş. Yalçin, D.R. Crosley, G.P. Smith, G.W. Faris. “Influence of ambient conditions on the laser air spark”, Appl. Phys. B 68, 121–130 (1999). DOI:https://doi.org/10.1364/LACEA.1996.LWA.2
55. A. Bartnik, V.M. Dyakin, P. Parys, I.Y. Skobelev, A.Y. Faenov, H. Fiedorowicz, S.Y. Khakhalin, “Investigation of an X-ray source based on a gas puff heated by laser radiation”. Quantum Electron. 25, 19 (1995). DOI:10.1070/QE1995v025n01ABEH000276

56. J. Jasik, J. Heitz, J. D. Pedarnig, P. Veis, “Vacuum ultraviolet laser-induced breakdown spectroscopy analysis of polymers”., Spectrochim. Acta Part B 64, 1128–1134 (2009). DOI: https://doi.org/10.1016/j.sab.2009.07.013
57. M.A. Gigosos, M.A. Gonzalez, V. Cardenoso, “Computer simulated balmer-alpha, -beta and -gamma stark line profiles for non-equilibrium plasmas diagnostics”, Spectrochim. Acta Part B 58, 1489–1504 (2003). DOI:https://doi.org/10.1016/S0584-8547(03)00097-1
58. S. K. Hussain Shah, J. Iqbal, P. Ahmad, M.U. Khandaker, S. Haq, M. Naeem, “Laser induced breakdown spectroscopy methods and applications: A comprehensive review”, Radiat. Phys. Chem. 170, 108666 (2020). DOI:https://doi.org/10.1016/J.RADPHYSCHEM.2019.108666
59. G. Cristoforetti, L. Antonelli, S. Atzeni, F. Baffigi, F. Barbato, D. Batani, G. Boutoux, A. Colaitis, J. Dostal, R. Dudzak, L. Juha, P. Koester, A. Marocchino, D. Mancelli, Ph. Nicolai, O. Renner, J. J. Santos, A. Schiavi, M. M. Skoric, M. Smid, P. Straka, L. A. Gizzi. “Measurements of parametric instabilities at laser intensities relevant to strong shock generation”, Phys. Plasmas 25, 012702 (2018). DOI:https://doi.org/10.1063/1.5006021
60. S. T. Lin and A. M. Ronn, “Laser induced sulfur particulate formation”, Chem. Phys. Lett. 56, 414-418 (1978). DOI:https://doi.org/10.1016/0009-2614(78)89005-8
61. A. S. Mahdi, Z. Abdul-Malek, and R. N. Arshad, “SF_6 decomposed component analysis for partial discharge diagnosis in GIS: A review”, IEEE Access 10, 27270-27288 (2022). DOI:https://doi.org/10.1109/ACCESS.2022.3156926
62. A. A. Opalovskij and Je. U. Lobkov: “Sulphur hexafluoride”, Usp. Khimii 46, 193-213 (1975).
63. T. Kiang, R. N. Zare: “Stepwise bond dissociation energies in sulfur hexafluoride”, J. Am. Chem. Soc., 102, 4024–4029 (1980). DOI:https://doi.org/10.1021/ja00532a008
64. M. Yang, J. Yan, M. Xu, Y. Geng, Zh. Liu, and J. Wang: “Study of the mechanisms of the temperature on the decomposition reaction of SF_n (n=1-6) under discharge conditions”, J. Mol. Model. 27, 236 (2021). DOI:https://doi.org/10.1007/s00894-021-04866-2
65. M. Miletic, O. Neškovic, M. Veljkovic, K. F. Zmbov: “Mass spectrometric study of the ionization and dissociation of sulphur hexafluoride by monoenergetic electron impact”, Rapid Commun. Mass Spectrom. 12, 753–758 (1998). DOI:

https://doi.org/10.1017/hpl.2025.10061 Published online by Cambridge University Press

https://doi.org/10.1002/(SICI)1097-0231(19980630)12:12%3C753::AID-RCM227%3E3.0.CO;2-Z

66. D. K. Padma and A. R. Vasudeva Murthy, “Thermal decomposition of sulphur hexafluoride”, Journal of Fluorine Chemistry 5,181-184 (1975). DOI:https://doi.org/10.1016/S0022-1139(00)81706-6
67. A. V. Eletskii, V. D. Klimov, and V. A. Legasov, “Mechanism of decomposition of inorganic fluorides in optical-breakdown plasmas caused by pulsed CO_2-laser radiation”, High Energy Chemistry 13, 388-391 (1979).
68. D. Babánková, S. Civiš, L. Juha: “Chemical consequences of laser-induced breakdown in molecular gases”, Prog. Quant. Electron. 30, 75-88 (2006). DOI: https://doi.org/10.1016/j.pquantelec.2006.09.001
69. L. Juha, S. Civiš, *Laser-plasma chemistry: Chemical reactions initiated by laser-produced plasmas*, In: Lasers in Chemistry (Ed. M. Lackner, Vol. 2, Wiley-VCH, Weinheim 2008), pp. 899-921.

https://doi.org/10.1017/hpl.2025.10061 Published online by Cambridge University Press

Figures

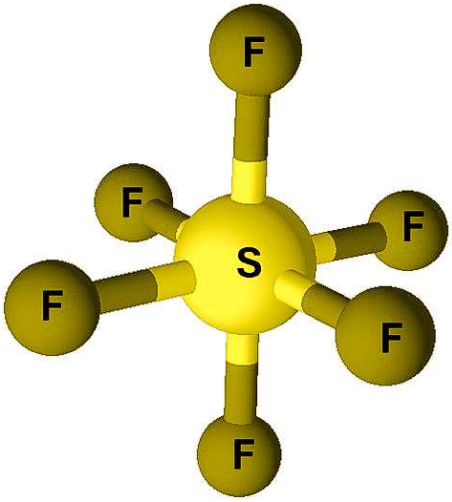

Figure 1 Ball and stick model of sulphur hexafluoride.

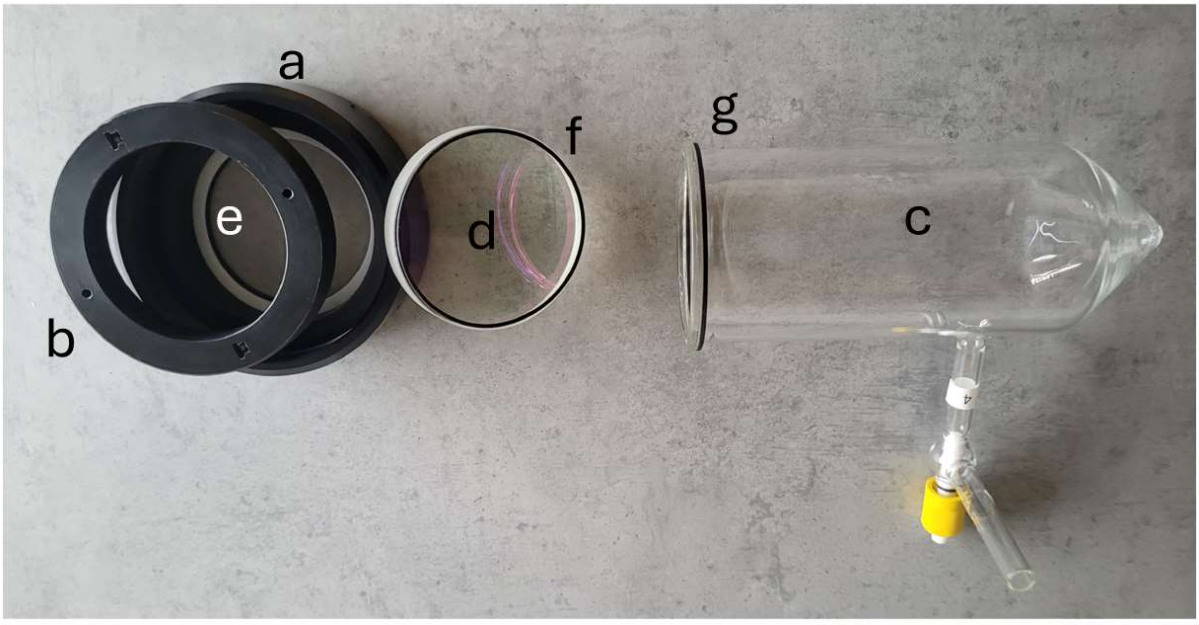

Figure 2 Gas cell - Murytal® flanges: (a) front part; (b) rear part composed of two pieces; (c) glass body of the cell; (d) BK7 window with antireflective coating; (e) Teflon® gasket; (f) Kalrez® O-ring; (g) NBR rubber gasket.

https://doi.org/10.1017/hpl.2025.10061 Published online by Cambridge University Press

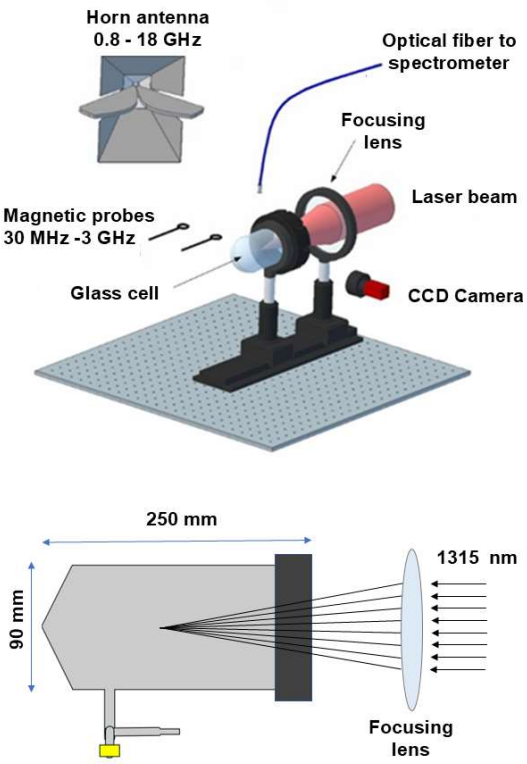

Figure 3 Schematic of experimental setup: (top) A diagram showing a cell, focusing length and a position of the detectors used. Drawing of the cell: (bottom) The image below shows a drawing that describes its dimensions including a lens focusing a light into the center of the gas cell.

https://doi.org/10.1017/hpl.2025.10061 Published online by Cambridge University Press

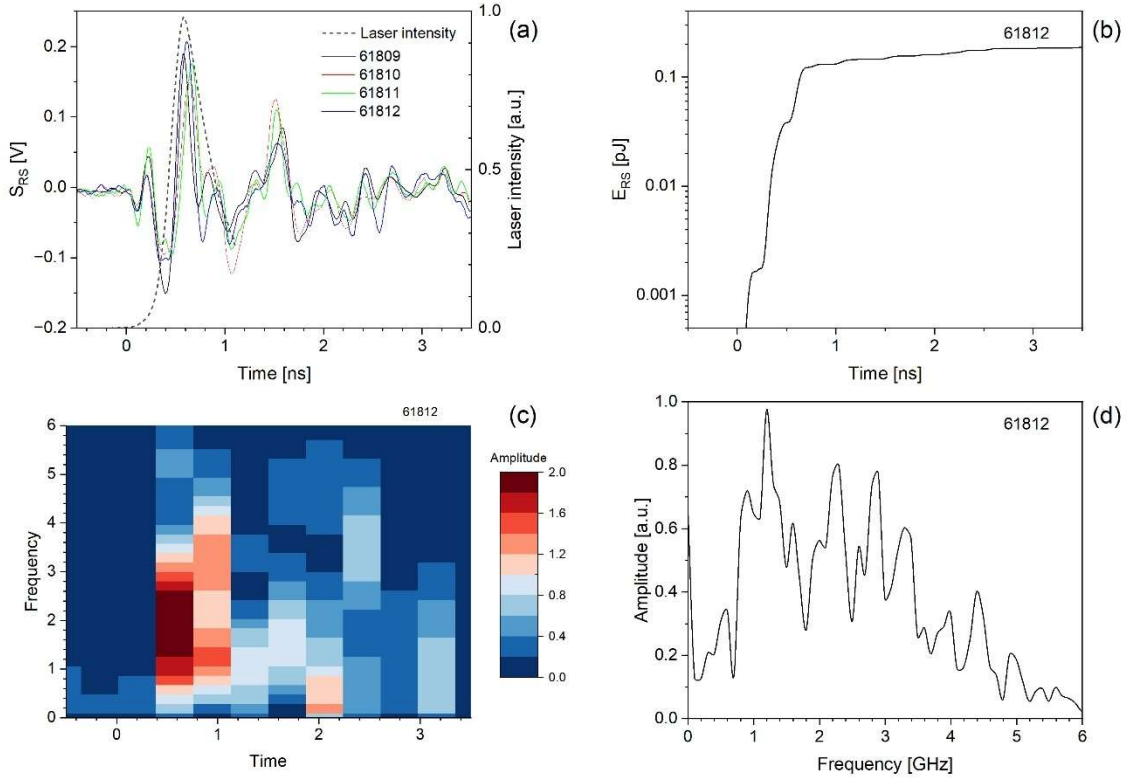

Figure 4 Electromagnetic radiation detected with the use of the magnetic probe localised 10 cm from the laser spark induced by a 350ps, 125J laser pulse focused into a cell filled with 53.3 kPa SF_6. (a) Correlation of the relative laser intensity (right Y scale) with the first positive peak of S_{RS} signals of the magnetic probe which were recorded at different shots, (b) energy absorbed by the loop probe at the shot 61812, (c) STFT of S_{RS} for shot 61812, (d) S_{RS} frequency spectra for shot 61812.

https://doi.org/10.1017/hpl.2025.10061 Published online by Cambridge University Press

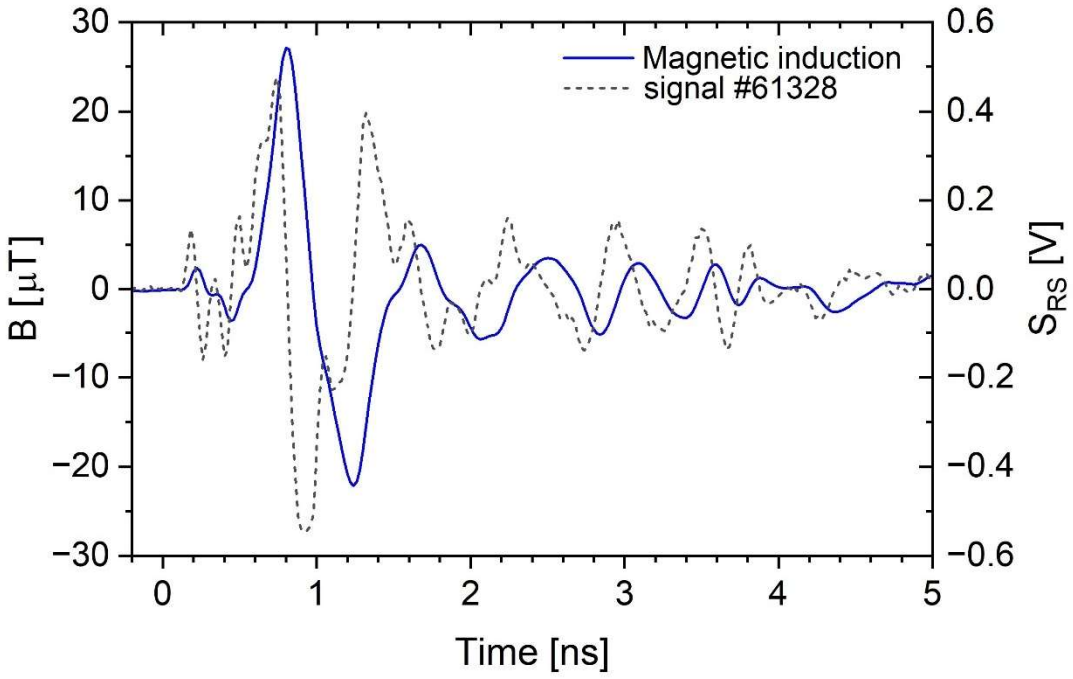

Figure 5 S_{RS} signal and its integral $\int_0^t S_{RS}(t)dt$. SF_6 pressure of 26.7 kPa.

https://doi.org/10.1017/hpl.2025.10061 Published online by Cambridge University Press

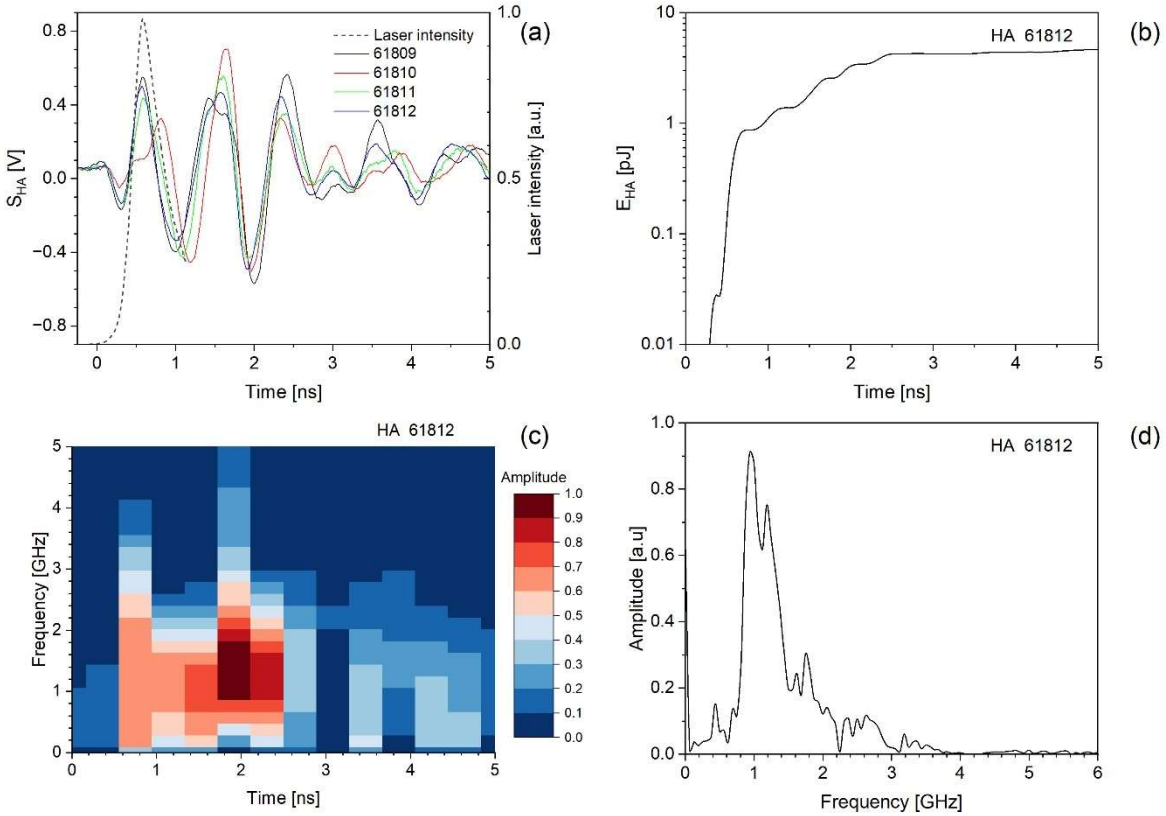

Figure 6 EMP induced by a single 350-ps, 125-J laser pulse focused into a cell filled with 53.3 kPa SF_6. (a) Correlation of the relative laser intensity, I_L, with the first positive peak of S_{HA} signals recorded at different shots, (b) Energy absorbed by HA for shot 61812, (c) STFT of S_{HA} for shot 61812, (d) S_{HA} frequency spectra for shot 61812.

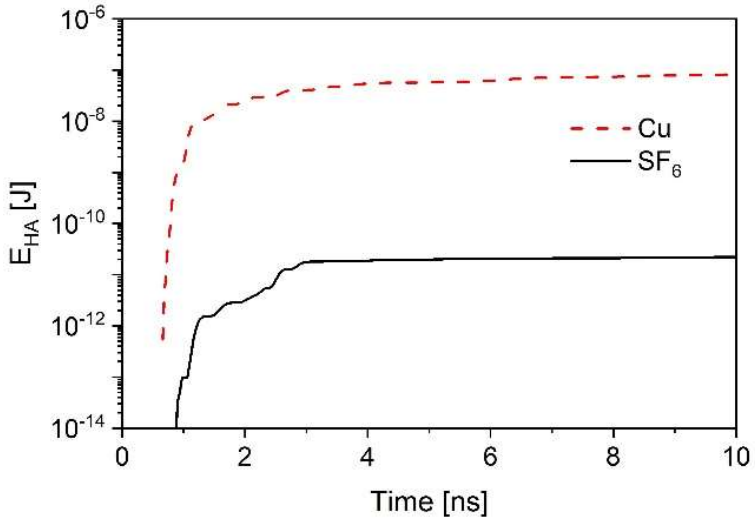

https://doi.org/10.1017/hpl.2025.10061 Published online by Cambridge University Press

Figure 7 Comparison of energy absorbed by HA detecting EMP produced by the interaction of a 150 J laser pulse with a 1mm thin Cu target and SF_6 gas at a pressure of 101.3 kPa.

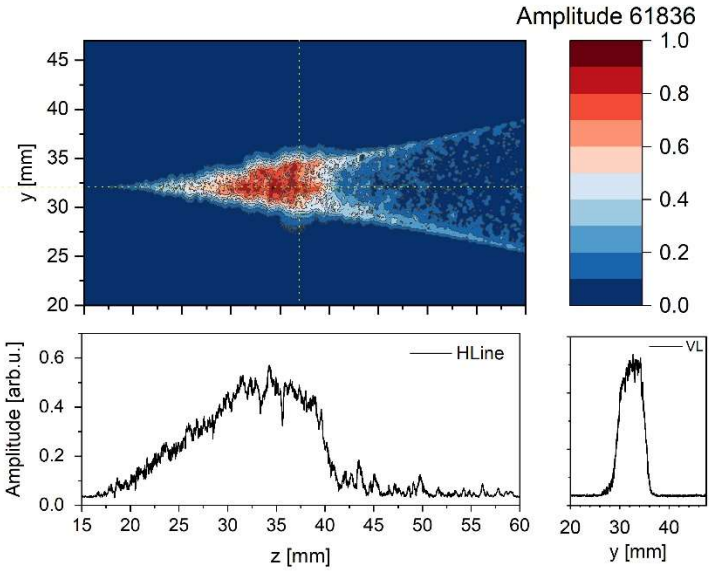

Figure 8 Passive laser spark imaging due to LIDB plasma optical emission. The longitudinal (Hline) and radial profiles (VL) of the spark's luminosity were extracted at the locations marked by the yellow lines in the diagram. Red arrows indicate the focused breakdown laser beam.

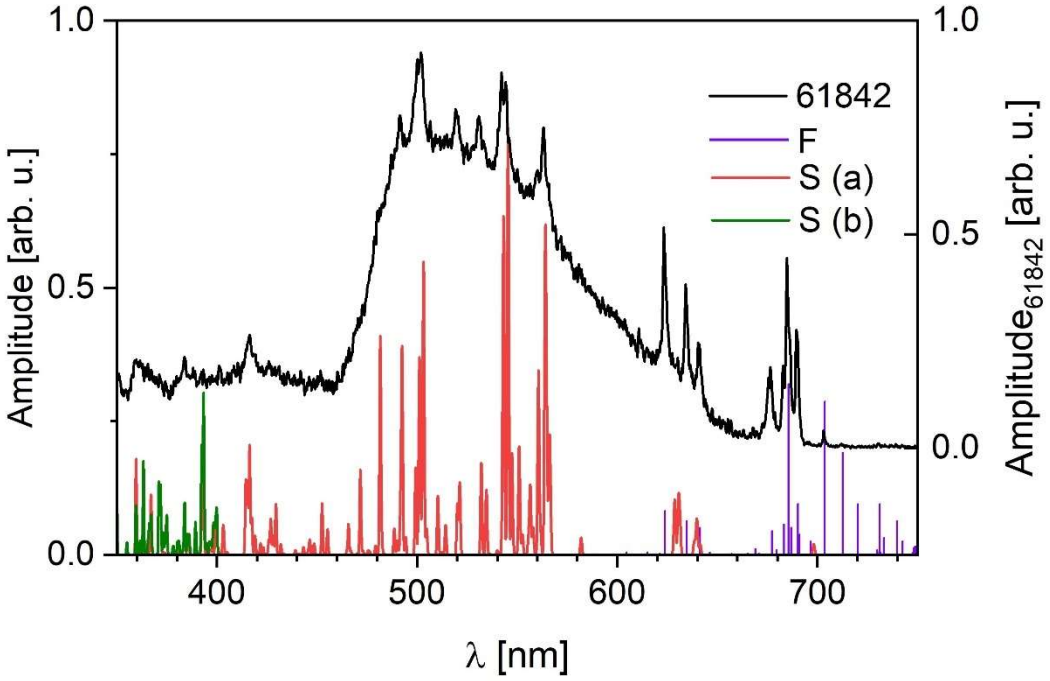

Figure 9 Optical emission spectra of laser sparks produced in SF_6. (101.3 kPa, 133 J) and fit of sulphur (a) S II lines at T_e=0.9 eV and n_e=1×10^{11} cm^{-3}, (b) S III at T_e=2.2 eV and n_e=1×10^{17} cm^{-3} and fluorine lines F I at T_e=0.9 eV and n_e=1×10^{14} cm^{-3} and background signal (BS).

https://doi.org/10.1017/hpl.2025.10061 Published online by Cambridge University Press

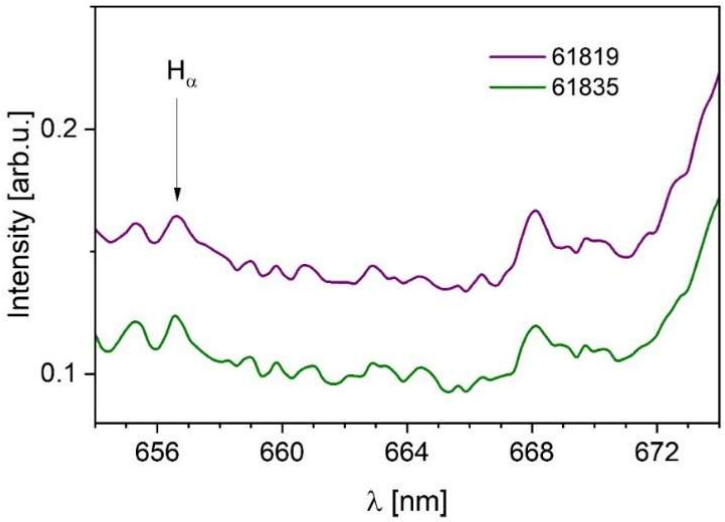

Figure 10 Detail of optical emission spectra of laser sparks produced in SF_6 at 101.3 kPa. The arrow indicates the wavelength of the H_α spectral line.

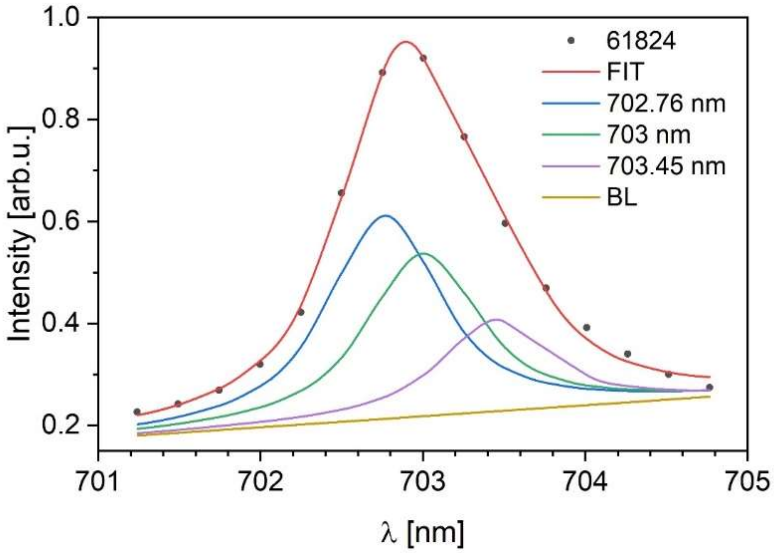

Figure 11 Detail of optical emission spectra of laser sparks produced in SF_6 at 26.7 kPa. The peak corresponds to the S V triplet at 702.76, 703.00, and 703.45 nm.

https://doi.org/10.1017/hpl.2025.10061 Published online by Cambridge University Press

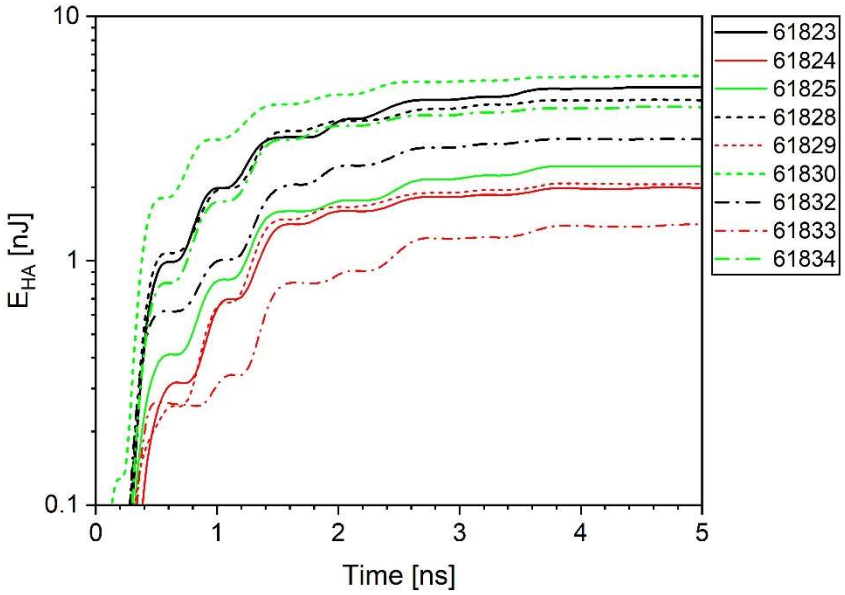

Figure 12 Time course of the energy of the horn antenna signal induced by EMP emitted from laser spark produced in SF_6 at 26.7 kPa, E_L ~ 125±7 J.

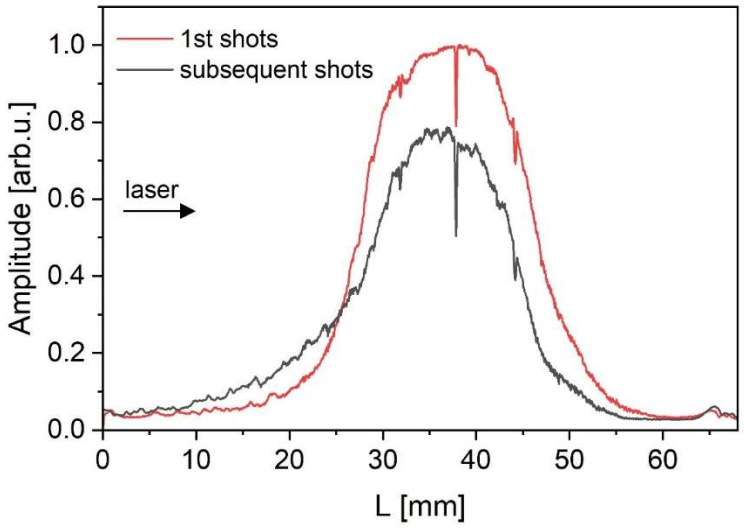

Figure 13 Intensity profile along the caustic line evaluated from spark photographs. The profiles shown are averages of the intensities obtained over three series of shots at SF_6 pressure of 26.7 kPa, E_L ~ 125±7 J.

https://doi.org/10.1017/hpl.2025.10061 Published online by Cambridge University Press

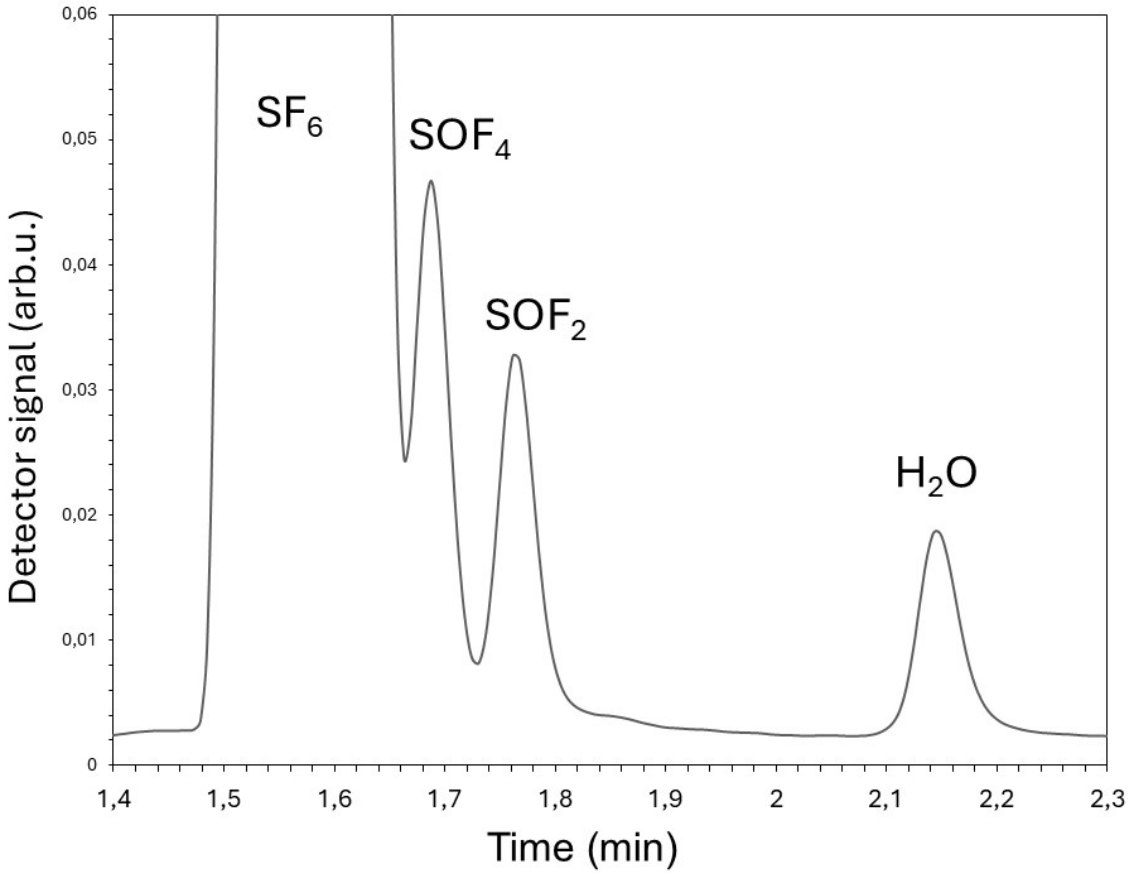

Figure 14 The gas chromatogram of SF_6 (containing traces of moist air) chemically altered by LIDB plasmas induced by four laser pulses focused into the gas cell (a total pressure in the cell is of 10.7 kPa) shot by shot.

https://doi.org/10.1017/hpl.2025.10061 Published online by Cambridge University Press